Mineralogical Magazine, December 2012, Vol. 76(8), pp. 3095–3104

Uranium uptake onto Magnox sludge minerals studied using EXAFS

A. VAN VEELEN[1], R. COPPING[2], G. T. W. LAW[3], A. J. SMITH[1], J. R. BARGAR[4], J. ROGERS[4], D. K. SHUH[2] AND R. A. WOGELIUS[1,*]

[1] University of Manchester, School of Earth, Atmospheric and Environmental Sciences, Oxford Road, Manchester, M13 9PL, UK
[2] Chemical Sciences Division, Lawrence Berkeley National Laboratory, MS70A1150, One Cyclotron Road, Berkeley, California 94720, USA
[3] University of Manchester, Centre for Radiochemistry Research, School of Chemistry, Oxford Road, Manchester, M13 9PL, UK
[4] Stanford Synchrotron Radiation Lightsource, PO Box 4349, Stanford, California 94309, USA

[*Received 19 December 2011; Accepted 12 June 2012; Associate Editor: Nicholas Evans*]

ABSTRACT

Around the world large quantities of sludge wastes derived from nuclear energy production are currently kept in storage facilities. In the UK, the British government has marked sludge removal as a top priority as these facilities are nearing the end of their operational lifetimes. Therefore chemical understanding of uranium uptake in Mg-rich sludge is critical for successful remediation strategies. Previous studies have explored uranium uptake by the calcium carbonate minerals, calcite and aragonite, under conditions applicable to both natural and anthropogenically perturbed systems. However, studies of the uptake by Mg-rich minerals such as brucite [$Mg(OH)_2$], nesquehonite [$MgCO_3{\cdot}3H_2O$] and hydromagnesite [$Mg_5(CO_3)_4(OH)_2{\cdot}4H_2O$], have not been previously conducted. Such experiments will improve our understanding of the mobility of uranium and other actinides in natural lithologies as well as provide key information applicable to nuclear waste repository strategies involving Mg-rich phases. Experiments with mineral powders were used to determine the partition coefficients (K_d) and coordination of UO_2^{2+} during adsorption and co-precipitation with brucite, nesquehonite and hydromagnesite. The K_d values for the selected Mg-rich minerals were comparable or greater than those published for calcium carbonates. Extended X-ray absorption fine structure analysis results showed that the structure of the uranyl-triscarbonato [$UO_2(CO_3)_3$] species was maintained after surface attachment and that uptake of uranyl ions took place mainly via mineral surface reactions.

KEYWORDS: hydromagnesite, nesquehonite, magnesium carbonates, Magnox sludge waste remediation.

Introduction

LARGE quantities of sludge wastes derived from nuclear power are currently housed in storage facilities around the world. In the UK, over 1000 m^3 of radioactive waste from the first generation Magnox fuel cans are currently stored under water at high pH (>11) at the Sellafield facility (Daniel and Acton, 2006; Hastings *et al.*, 2007). Magnox is the industrial name for the Mg/Al alloy fuel cladding (the name signifies 'magnesium, non-oxidizing'). During its operational service, Sellafield's Magnox Storage and De-canning Facility (MSDF) reprocessed 27,000 t of fuel (Topping and Bruce, 2006). However, during the mid-1970s significant clean-up challenges were created. Most importantly, spent fuel was stored

* E-mail: roy.wogelius@manchester.ac.uk
DOI: 10.1180/minmag.2012.076.8.24

in the ponds for longer than the designed period. As a result the fuel cladding became extensively corroded and instead of an easy removal of the fuel rods from the cladding, a complex and highly contaminated waste has been produced. Additionally, in the absence of waste management, significant amounts of intermediate-level waste have accumulated creating some of the most complex radiological remediation and clean up challenges in the world (Topping and Bruce, 2006). Moreover, limited records exist of what exactly was stored in these facilities, due to changing priorities at the time (Horsley and Hallington, 2005).

The British government has marked sludge removal and reprocessing as a top priority. With the ponds approaching their end of their design life, waste retrieval and decommissioning strategies are essential (Hastings *et al.*, 2007). Characterization and understanding of the sludge's behaviour is critical, as geological disposal is the final goal. Its heterogeneous nature, potential for solid/liquid separation, and poorly understood chemistry all create difficulties in formulating a remediation strategy. In fact, there is limited information available of the composition of the sludge, except for the likelihood that magnesium hydroxides and magnesium carbonates appear to dominate. In this contribution, uptake experiments of uranium onto three mineral powders are described.

Uranium in solution

Uranium is the most common radionuclide contaminant in soils and groundwaters and is one of the most toxic elements (Schindler and Putnis, 2004). There is a real need for information concerning actinide speciation (Denecke, 2006). This importance stems from the fact that whatever form the nuclide takes has an influence on the solubility, mobility, bioavailability, toxicity and consequently risk for human health. In water and in contact with air, uranium exists predominantly in the U(VI) oxidation state as the (UO_2^{2+}) uranyl cation (Hudson *et al.*, 1999), which is very mobile compared to the U(IV) oxidation state. The U(VI) state readily forms complexes with several naturally occurring organic ligands which are known to increase its environmental mobility (Clark *et al.*, 1995; Bargar *et al.*, 1999; Schindler and Putnis, 2004; Denecke, 2006). Changes in U(VI) speciation, temperature and solution composition all affect the attachment of uranyl to the solid phase and thereby control its mobility. As a consequence, a knowledge of the probable speciation in the aqueous phase enables us to predict how uranyl will attach to magnesium-bearing mineral surfaces and eventually partition into bulk solids.

Previous studies have shown that the uranyl triscarbonato $(UO_2(CO_3)_3)^{4-}$ species will dominate at pH greater than 9 (Clark *et al.*, 1995; Greathouse and Cygan, 2005). In the cooling ponds, the fluid pH is kept above pH 9 and in some cases adjusted to pH 13 (Daniel and Acton, 2006) to prevent dissolution of the Magnox. The high pH causes atmospheric CO_2 to dissolve readily, especially in these open air fluids, meaning that carbonate complexation is an important consideration in understanding these sludge compositions. Uranyl, in these circumstances, forms strong complexes with CO_3^{2-} anions.

Uranium in carbonates

Sorption of uranium onto calcite has been well studied (Reeder *et al.*, 2000; Kelly *et al.*, 2003, 2006) but research on uranyl uptake in magnesium-bearing minerals such as magnesite [$MgCO_3$], nesquehonite [$MgCO_3{\cdot}3H_2O$] and hydromagnesite [$Mg_5(CO_3)_4(OH)_2{\cdot}4H_2O$] has not, to the best of our knowledge, been previously conducted. The Mg–O bond distances in magnesite (2.082 Å) are shorter than Ca–O in calcite (2.35 Å). Total distortion of the octahedral site in calcite is much greater compared to magnesite (Finch and Allison, 2007). However, the shorter bond distance for Mg could be interpreted to indicate that partition coefficients of uranyl into magnesite might be lower compared to those for calcite.

Uptake of uranium is dependent on the structure of the carbonate mineral (Sturchio *et al.*, 1998; Reeder *et al.*, 2000, 2001). Uranyl is preferentially incorporated into metastable aragonite [$CaCO_3$] (orthorhombic) relative to calcite (rhombohedral). The incorporation of uranyl in calcite has been debated due to the size and shape of the linear uranyl moiety $(O{=}U{=}O)^{2+}$, which is considerably different from that of Ca^{2+} for which it substitutes (Russell *et al.*, 1994). Moreover, the structure of rutherfordine [$UO_2(CO_3)$] is orthorhombic (Christ *et al.*, 1955), which is more similar to aragonite. Additionally, chemical data, from both experimental and analytical studies, indicates that uranyl behaves as a dilute solid

https://doi.org/10.1180/minmag.2012.076.8.24 Published online by Cambridge University Press

solution in aragonite and calcite (Russell *et al.*, 1994). The solid-solution distribution coefficients measured for uranyl in aragonite are an order of magnitude higher than that for uranyl into calcite, indicating that aragonite is more compatible with uranyl substitution than calcite (Kelly *et al.*, 2003). Incorporation of uranyl in the calcite structure will significantly disorder the structure, which suggests a less stable final structure (Reeder *et al.*, 2001).

Uranium attached on the surface

Uranium incorporation mainly takes place at the mineral surface (Geipel *et al.*, 1997). Surface specific information about active sites where adsorption takes place is important for making predictions about how uranyl is incorporated. A study using polarized extended X-ray absorption fine structure (EXAFS) analysis to study uranyl adsorption on the basal plane of montmorillonite showed outer sphere complexation to dominate and concluded no orientation information could be extracted (Greathouse *et al.*, 2005). In contrast, polarized EXAFS results of uranyl adsorption onto α-Al_2O_3 indicated a bidentate cation binding onto the surface exposed oxygen atoms in such way that the uranyl axis was parallel to the surface at a distance of 1.76 Å from two surface oxygen atoms (Denecke *et al.*, 2003).

Identification of the minerals composing the sludge, in combination with a detailed physical and chemical understanding of the bulk coordination chemistry of the radionuclides are both necessary to predict the transport of released radionuclides into the environment (Denecke, 2006). Therefore in this study a laboratory bulk adsorption experiment of uranyl onto brucite [$Mg(OH)_2$] and onto the metastable carbonate phases nesquehonite [$MgCO_3{\cdot}3H_2O$] and hydromagnesite [$Mg_5(CO_3)_4(OH)_2{\cdot}4H_2O$] was carried out. Conditions were kept similar to that within the ponds at Sellafield (i.e. at basic pH, at ambient temperature, and with carbonate available in the reactant solutions). Synthesized reactant solids were characterized using X-ray diffraction (XRD). The amount of uranium that was taken up by the solid phase after reaction was determined by the difference between inductively-coupled plasma atomic emission spectroscopy (ICP-AES) analysis of the product and reactant fluids. Finally, the coordination chemistry of the uranium within the product solids was analysed at the uranium L_{III}-edge using EXAFS analysis. The goals of this study are: (1) to determine the extent of uranium adsorption onto these solid phases through bulk solution analysis; and (2) to provide information on how uranium is bonded to these surfaces by using EXAFS. The findings of this study provide valuable information on the behaviour of the actinides.

Experimental

Mineral synthesis

The brucite, nesquehonite and hydromagnesite powders used in these experiments were synthesized from $MgCl_2{\cdot}6H_2O$ following the methodologies described in Hänchen *et al.* (2008). Brucite was synthesized at 25ºC under CO_2 free conditions. Nesquehonite was synthesized at 25ºC by adding 0.6 mol kg^{-1} Na_2CO_3 to a stock magnesium chloride solution under 0.2 atm P_{CO2} in sealed reactors. Precipitates were filtered and dried at 60ºC for 12 h. To form hydromagnesite, the nesquehonite precipitates were placed in a reaction vessel above 20 g of dry ice and placed in an oven at 75ºC for 12 h. These procedures have been reported to produce clean brucite, nesquehonite and hydromagnesite surfaces. Analyses by XRD showed the products to be crystalline brucite, nesquehonite and hydromagnesite.

Reaction with uranium

Adsorption

A stock solution of 0.1 M U(VI) was prepared from an isotopically depleted $UO_2^{2+}(NO_3)_2{\cdot}6H_2O$ source. The adsorption experiments were designed in such way that wherever possible the total U(VI) present would be more than the solubility of crystalline schoepite [$(UO_2)_8O_2(OH)_{12}{\cdot}12H_2O$]. To produce the final stock solution concentrations of 500 and 50 ppm U(VI), 1.05 and 0.105 ml of stock solution were diluted in 50 ml deionized water. Prior to the dilution of uranyl, 2.0 mM of Na_2CO_3 was added to improve solubility. The pH of the solutions were adjusted drop-wise using NaOH to pH 8.25.

For reaction the synthesized powders were transferred into 25 ml Falcon tubes and then reactant fluids were added. The ratio of sample to solution was 1:30. Contact time was ~48 h (±1 h) after which the samples were centrifuged using an IEC Clinical Centrifuge at 5000 rpm (4500–5000 g). The supernatant was decanted and the removal of water from the wet solids was accelerated by brief exposure to partial vacuum.

https://doi.org/10.1180/minmag.2012.076.8.24 Published online by Cambridge University Press

Co-precipitation

For comparison to the adsorption experiments, a single experiment was completed to determine uranyl uptake into brucite as it was allowed to precipitate from a supersaturated solution. In this case, brucite was synthesized following the methodology described above, however once a steady-state pH was achieved during precipitate formation 2 ml of 100 mM uranyl nitrate hexahydrate stock was added to the solution. The pH of the solution was then maintained at 10.07 via the incremental addition of 0.01 M NaOH to the solution. The final uranium concentration of this solution was 640 ppm. Brucite precipitates were allowed to form for approximately one hour. The solution was then centrifuged at 300 rpm and precipitates were filtered from the supernatant using 30 μm filter paper. Precipitates were rinsed with deionized water to dissolve any halite or other impurities and mixed with deionized water within a centrifuge tube and centrifuged for a final time. Precipitates were again filtered. The precipitate was then allowed to dry in a temperature controlled oven at a constant temperature of 40ºC.

EXAFS measurements

The EXAFS measurements were performed at beamline 11-2 at the Stanford Synchrotron Radiation Lightsource (SSRL) of the SLAC National Accelerator Laboratory, USA. This beamline was specially set up for such experiments. The energy of the beam was calibrated against the first derivative of a Y foil, defined as 17,038 eV. The measurements were conducted in transmission mode. The EXAFS data were collected for all mineral products except the 50 ppm nesquehonite sample, which could not be measured due to time constraints.

The EXAFS, $\chi(k)$, were isolated from raw data by the standard procedures (background subtraction, normalization of absorption, conversion to momentum, k, space). For each sample six spectra were averaged in order to improve signal to noise ratio. The spectra were analysed with *SixPack* and phase/amplitude functions calculated with *FEFF6L*. Theoretical fits were performed in R-space.

Results and discussion

Synthesized minerals

The protocols developed for synthesizing the minerals brucite, nesquehonite and hydromagnesite were successful and their powder patterns were verified by XRD (Fig.1). An examination of the synthesized nesqhuehonite pattern suggested that poorly crystalline artinite [$Mg_2CO_3(OH)_2 \cdot 3H_2O$] (reference pattern: JCP-01-070-0591) may be present as a minor fraction. Only the most intense artinite peak ($\bar{2}01$) could be resolved; the peak width relative to the nesquehonite peaks suggested it to be poorly crystalline, and the relatively low intensity indicates a minor component of the synthesized solid. The quality of the hydromagnesite powder pattern is slightly poorer than the other phases, potentially due to inclusions or small domains of $MgCO_3$ or $Mg(OH)_2$ within the powder. However, the quality and purity of the powders is good and the XRD patterns of the synthesized minerals are in good agreement with the known peak positions of standard reference patterns for these minerals. These results indicate that the developed protocols are successful for the preparation of stable and metastable Mg-bearing minerals.

Adsorption experiments

The K_d values determined from the reactions between the magnesium mineral powders and uranyl-bearing fluids are shown in Table 1. Although this empirical model is extremely limited in terms of predictive power (Vaughan and Wogelius, 2000), it still gives valuable information in a simplified system containing a single mineral, an aqueous phase, and a single sorbate. These K_d values also may be conveniently compared to other similar experimental adsorption data. In addition, the results obtained here detailing surface atomic configurations may be used in more complicated adsorption models. All solids showed higher K_d values than those previously determined for calcite [Kelly *et al.* (2003); representative K_d = 4.3 ml g^{-1}]. In these experiments the highest K_d value was observed as expected for the brucite co-precipitated in the presence of 640 ppm uranium. The other K_d values represent simple adsorption onto a single mineral phase. Again, the highest values were obtained for brucite, whereas nesquehonite and hydromagnesite produced similar results to each other. These results suggest that uranyl binding is optimized on the magnesium hydroxide mineral surfaces relative to the carbonates.

The XRD results showed no significant peak shifts between the pure minerals and the post-sorption minerals. Peak shifts might be particularly important if uranyl were incorporated

https://doi.org/10.1180/minmag.2012.076.8.24 Published online by Cambridge University Press

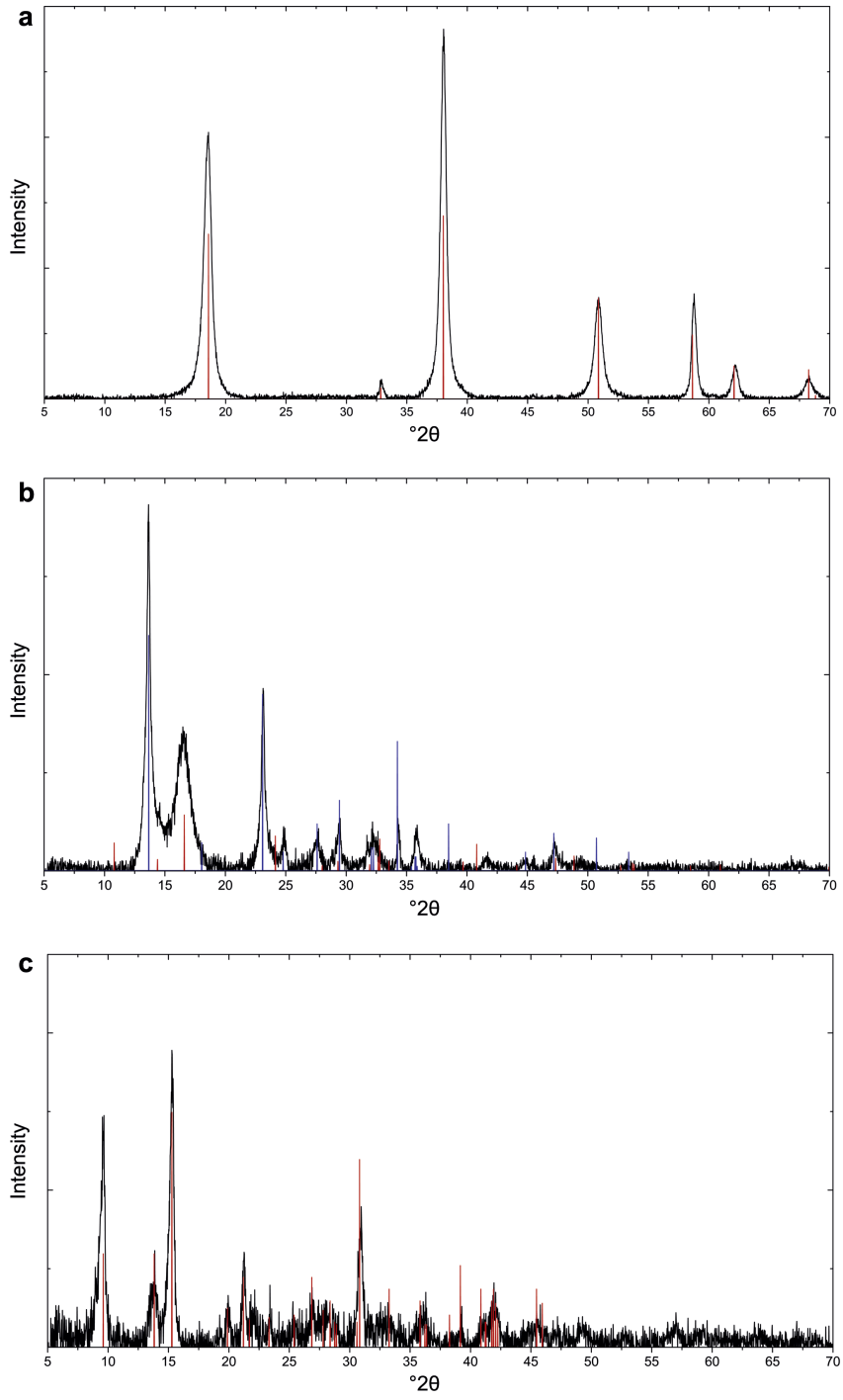

FIG. 1. Data from the X-ray diffraction analysis. (*a*) Brucite (reference pattern in red: JCP-00-007-0239). (*b*) Nesquehonite (reference pattern in blue: JCP-00-020-0669) with minor artinite (reference pattern in red: JCP-010-070-0591). (c) Hydromagnesite (reference pattern in red: JCP-00-025-0513).

https://doi.org/10.1180/minmag.2012.076.8.24 Published online by Cambridge University Press

TABLE 1. Summary of U(VI) adsorption on Mg solids.

Sample description	Mass solid (g)	Volume (ml)	K_d*
Brucite with 640 ppm U(VI)	0.933	50	53.5
Brucite with 500 ppm U(VI)	0.101	3	23
Brucite with 50 ppm U(VI)	0.21	6	10.6
Hydromagnesite with 500 ppm U(VI)	0.211	6	13.4
Hydromagnesite with 50 ppm U(VI)	0.21	6	7.5
Nesquehonite with 500 ppm U(VI)	0.106	3	15.1
Nesquehonite with 50 ppm U(VI)**	0.106	3	6.8

* K_d is the partition coefficient.
** EXAFS data are not available for this sample

between the brucite octahedral layers which would distort the basal plane distance (Hudson *et al.*, 1999). Our diffraction results suggest that the brucite basal plane spacing is not significantly distorted and this implies either that most U(VI) is not concentrated within the interlayer or, less probably, that U(VI) is somehow incorporated with minimal structural distortion.

The EXAFS analyses

The radial distribution functions (RDF, Fourier transform magnitudes) with their corresponding fits analysed by EXAFS are shown in Fig. 2. The data for all the samples reacted at different concentrations all resemble reference spectra of uranyl triscarbonato complexes. In addition, the EXAFS spectra show remarkable similarities with earlier published spectra for U(VI) adsorption onto calcite (Elzinga *et al.*, 2004).

All spectra show two well resolved oxygen features, one for the axial and one for the equatorial oxygen atoms. However, the spectrum of brucite co-precipitated with uranyl nitrate is different, with one well resolved peak and a weaker broader peak, probably due to its less well ordered crystallographic structure. Fits of the RDF resulted in 7−8 oxygen atoms, 2 for the axial uranyl oxygen atoms and 5−6 for the equatorial oxygen atoms. The position of the axial oxygen feature, at R ~1.81 Å, is consistent with all other samples, which indicates that the uranyl ion structure $(O{=}U{=}O)^{2+}$ is unaffected by precipitation within the brucite structure or through adsorption on the other magnesium solids. However, the equatorial oxygen shells (R ~2.35 Å) show an asymmetric feature at the higher R-side, indicating splitting in the equatorial shell for all but one sample. Shell-by-shell fits confirm this observation (Table 2).

Carbon atoms were resolved at slightly greater distance than the equatorial oxygen atoms. The third and fourth peaks in the RDF are resolved as Mg and U atoms. The amplitude of these peaks are lower, but are large enough to be resolved. In addition, three paths accounting for multiple scattering off of the $U{-}O_{ax}$ (at twice the distance) were included.

For all the reacted minerals, the EXAFS results show that the structure of the uranyl cation is maintained and it is not reduced to U(IV). All reacted synthesized minerals showed that uranium attaches onto the surface in a coordination polyhedron which strongly resembles uranyl triscarbonato $[UO_2(CO_3)_3^{4-}]$ complexes. Additionally the remarkable similarities between uranium adsorption on calcite and Mg-containing minerals, suggests that calcite is a good analogue for the adsorption of actinides onto Mg-containing minerals.

The similarities between all EXAFS spectra indicate that the adsorption of uranyl is comparable for all synthesized Mg-bearing minerals. In all spectra one Mg atom could be resolved, and in combination with the XRD results, this suggests that the U(VI) atoms are attached directly onto the surface of the minerals. Previous studies showed that U(VI) is attached as an outer-sphere complex with the uranyl axis parallel to the mineral surface of vermiculite, hydrobiotite (Hudson *et al.*, 1999), and calcite (Denecke *et al.*, 2005). It might be expected that uranyl would be adsorbed onto Mg mineral phases in a similar fashion. However, the nature of this experiment could not resolve the

https://doi.org/10.1180/minmag.2012.076.8.24 Published online by Cambridge University Press

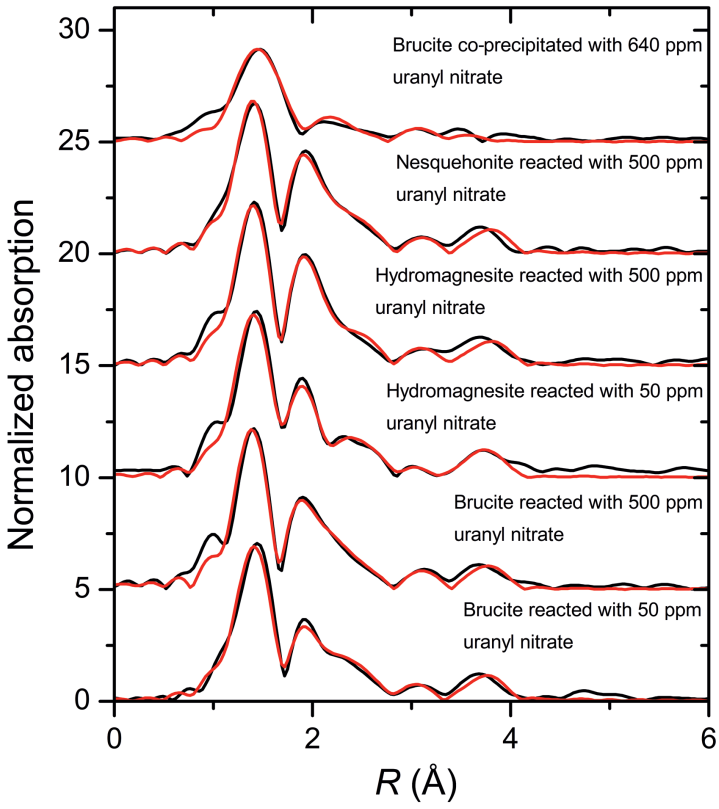

FIG. 2. Radial distribution functions (RDF, Fourier transform magnitude) of the synthesized minerals reacted with different loadings of U(VI).

exact orientation of the uranyl surface complex. Surface analysis using grazing incidence XAFS (GIXAFS) is proposed to resolve the adsorption and orientation of uranyl on these surfaces. In combination with the polarization dependence of the uranyl ion, as described in Hudson *et al.* (1996), the orientation and thus the way uranium is attached on the Mg mineral surface may be determined.

Conclusions

The goals of this study were to provide detailed information about three different aspects of Magnox sludge: (1) to test synthesis protocols for key Mg-rich phases; (2) to measure bulk partition coefficients of uranyl onto these minerals from basic solutions; and (3) to determine the coordination environment of attached uranyl. Results show that brucite and metastable carbonates can be reliably prepared. Furthermore, partitioning of uranyl onto magnesium hydroxides and carbonates exceeds that previously reported for calcium carbonates (Kelly *et al.*, 2003). Finally, EXAFS and XRD analyses show that uranium atoms are attached directly to the mineral surfaces with oxygen bond distances similar to those observed for $[UO_2(CO_3)_3^{4-}]$ (Allen *et al.*, 1995; Elzinga *et al.*, 2004), comparable to results with calcium carbonates reported in previous studies (Reeder *et al.*, 2000; Elzinga *et al.*, 2004). These results allow us to predict the mobility and partitioning of uranium during various processing scenarios of spent Magnox fuel. In addition, this work provides valuable insights into how actinides may react during transport through Mg-bearing backfill materials.

Acknowledgements

Arjen van Veelen is supported through the EPSRC/NDA Diamond nuclear consortium;

https://doi.org/10.1180/minmag.2012.076.8.24 Published online by Cambridge University Press

TABLE 2. Shell-by-shell fit parameters for L_{III}-edge EXAFS data for the uranyl containing brucite, hydromagnesite and nesquehonite samples.

Shell	*CN**	*R* (Å)†	σ^2 (Å^2)‡
Brucite reacted with 50 ppm uranyl nitrate			
U−Oax	2.290	1.815	0.00372
U−Oeq1	3.342	2.319	0.00872
U−Oeq2	3.459	2.459	0.00499
U–C	3.287	2.896	0.00220
U–Mg	1.262	3.599	0.00577
U–U	1.338	3.878	0.00508
Brucite reacted with 500 ppm uranyl nitrate			
U−Oax	1.606	1.804	0.00246
U−Oeq1	3.562	2.377	0.00836
U−Oeq2	1.447	2.475	0.00286
U–C	2.725	2.902	0.00349
U–Mg	1.072	3.600	0.00495
U–U	1.336	3.896	0.00652
Hydromagnesite reacted with 50 ppm uranyl nitrate			
U−Oax	2.348	1.801	0.00366
U−Oeq1	3.673	2.312	0.00914
U−Oeq2	2.811	2.414	0.00640
U–C	2.756	2.901	0.00101
U–Mg	1.449	3.567	0.00954
U–U	2.508	3.879	0.00792
Hydromagnesite reacted with 500 ppm uranyl nitrate			
U−Oax	2.157	1.813	0.00313
U−Oeq	5.545	2.426	0.00705
U–C	3.168	2.902	0.00303
U–Mg	1.859	3.619	0.00810
U–U	1.595	3.904	0.00610
Nesquehonite reacted with 500 ppm uranyl nitrate			
U−Oax	2.234	1.810	0.00327
U−Oeq1	4.381	2.395	0.00593
U−Oeq2	1.675	2.498	0.00317
U–C	3.857	2.903	0.00346
U–Mg	1.409	3.590	0.00536
U–U	1.624	3.887	0.00600
Brucite co-precipitated with 640 ppm uranyl nitrate			
U−Oax	1.840	1.824	0.00403
U−Oeq1	3.225	2.274	0.00700
U−Oeq2	2.094	2.469	0.00382
U–C	1.692	2.901	0.00459
U–Mg	0.556	3.594	0.00080
U–U	0.846	3.744	0.01533

Effects related to multiple scattering are included and important at ~3.6 Å.
* Coordination number.
† interatomic distance in Å.
‡ Debye−Waller factor.

https://doi.org/10.1180/minmag.2012.076.8.24 Published online by Cambridge University Press

G.T.W. Law was supported by NERC grant NE/H007768/1. Part of this work (R.C., D.K.S.) was supported by the Director, Office of Science, Office of Basic Energy Sciences, Division of Chemical Sciences, Geosciences, and Biosciences of the US Department of Energy (DOE) at Lawrence Berkeley National Laboratory under Contract No. DE-AC0205CH11231. Portions of this research were carried out at the Stanford Synchrotron Radiation Lightsource, a Directorate of SLAC National Accelerator Laboratory and an Office of Science User Facility operated for the U.S. DOE Office of Science by Stanford University. The SSRL Structural Molecular Biology Program is supported by the U.S. DOE Office of Biological and Environmental Research, and by the National Institutes of Health, National Center for Research Resources, Biomedical Technology Program (P41RR001209).

References

Allen, P.G., Bucher, J.J., Clark, D.L., Edelstein, N.M., Ekberg, S.A., Gohdes, J.W., Hudson, E.A., Kaltsoyannis, N., Lukens, W.W., Neu, M.P., Palmer, P.D., Reich, T., Shuh, D.K., Tait, C.D. and Zwick, B.D. (1995) Multinuclear NMR, Raman, EXAFS, and X-ray diffraction studies of uranyl carbonate complexes in near-neutral aqueous solution. X-ray structure of $[C(NH_2)_3]_6[(UO_2)_3(CO_3)_6]\cdot 6.5H_2O$. *Inorganic Chemistry*, **34**, 4797–4807.

Bargar, J.R., Reitmeyer, R. and Davis, J.A. (1999) Spectroscopic confirmation of uranium(VI)–carbonato adsorption complexes on hematite. *Environmental Science & Technology*, **33**, 2481–2484.

Christ, C.L., Clark, J.R. and Evans, H.T. (1955) Crystal structure of rutherfordine, UO_2CO_3. *Science*, **121**, 472–473.

Clark, D.L., Hobart, D.E. and Neu, M.P. (1995) Actinide carbonate complexes and their importance in actinide environmental chemistry. *Chemical Reviews*, **95**, 25–48.

Daniel, A.S. and Acton, R.A. (2006) Spent fuel management in the United Kingdom Pp. 57 in: *Scientific and technical issues in the management of spent fuel of decommissioned nuclear submarines* (A. Sarkisov, and A. Tournyol du Clos, editors). Springer, Dordrecht, The Netherlands.

Denecke, M.A. (2006) Actinide speciation using X-ray absorption fine structure spectroscopy. *Coordination Chemistry Reviews*, **250**, 730–754.

Denecke, M.A., Rothe, J., Dardenne, K. and Lindqvist-Reis, P. (2003) Grazing incidence (GI) XAFS measurements of Hf(IV) and U(VI) sorption onto mineral surfaces. *Physical Chemistry Chemical Physics*, **5**, 939–946.

Denecke, M.A., Bosbach, D., Dardenne, K., Lindqvist-Reis, P., Rothe, J. and Yin, R. (2005) Polarization dependent grazing incidence (GI) XAFS measurements of uranyl cation sorption onto mineral surfaces. *Physica Scripta*, **T115**, 877–881.

Elzinga, E.J., Tait, C.D., Reeder, R.J., Rector, K.D., Donohoe, R.J. and Morris, D.E. (2004) Spectroscopic investigation of U(VI) sorption at the calcite-water interface. *Geochimica et Cosmochimica Acta*, **68**, 2437–2448.

Finch, A.A. and Allison, N. (2007) Coordination of Sr and Mg in calcite and aragonite. *Mineralogical Magazine*, **71**, 539–552.

Geipel, G., Reich, T., Brendler, V., Bernhard, G. and Nitsche, H. (1997) Laser and X-ray spectroscopic studies of uranium–calcite interface phenomena. *Journal of Nuclear Materials*, **248**, 408–411.

Greathouse, J.A. and Cygan, R.T. (2005) Molecular dynamics simulation of uranyl(VI) adsorption equilibria onto an external montmorillonite surface. *Physical Chemistry Chemical Physics*, **7**, 3580–3586.

Greathouse, J.A., Stellalevinsohn, H.R., Denecke, M.A., Bauer, A. and Pabalan, R.T. (2005) Uranyl surface complexes in a mixed-charge montmorillonite: Monte Carlo computer simulation and polarized XAFS results. *Clays and Clay Minerals*, **53**, 278–286.

Hänchen, M., Prigiobbe, V., Baciocchi, R. and Mazzotti, M. (2008) Precipitation in the Mg-carbonate system – effects of temperature and CO_2 pressure. *Chemical Engineering Science*, **63**, 1012–1028.

Hastings, J.J., Rhodes, D., Fellerman, A.S., McKendrick, D. and Dixon, C. (2007) New approaches for sludge management in the nuclear industry. *Powder Technology*, **174**, 18–24.

Horsley, D.M.C. and Hallington, P.J. (2005) Nuclear power and the management of the radioactive waste legacy. *Chemical Engineering Research and Design*, **83**, 773–776.

Hudson, E.A., Allen, P.G., Terminello, L.J., Denecke, M.A. and Reich, T. (1996) Polarized X-ray-absorption spectroscopy of the uranyl ion: comparison of experiment and theory. *Physical Review B*, **54**, 156–165.

Hudson, E.A., Terminello, L.J., Viani, B.E., Denecke, M., Reich, T., Allen, P.G., Bucher, J.J., Shuh, D.K. and Edelstein, N.M. (1999) The structure of U6+ sorption complexes on vermiculite and hydrobiotite. *Clays and Clay Minerals*, **47**, 439–457.

Kelly, S.D., Newville, M.G., Cheng, L., Kemner, K.M., Sutton, S.R., Fenter, P., Sturchio, N.C. and Spötl, C. (2003) Uranyl incorporation in natural calcite.

Environmental Science & Technology, **37**, 1284–1287.

Kelly, S.D., Rasbury, E.T., Chattopadhyay, S., Kropf, A.J. and Kemner, K.M. (2006) Evidence of a stable uranyl site in ancient organic-rich calcite. *Environmental Science & Technology*, **40**, 2262–2268.

Reeder, R.J., Nugent, M., Lamble, G.M., Tait, C.D. and Morris, D.E. (2000) Uranyl incorporation into calcite and aragonite: XAFS and luminescence studies. *Environmental Science & Technology*, **34**, 638–644.

Reeder, R.J., Nugent, M., Tait, C.D., Morris, D.E., Heald, S.M., Beck, K.M., Hess, W.P. and Lanzirotti, A. (2001) Coprecipitation of uranium(VI) with calcite: XAFS, micro-XAS, and luminescence characterization. *Geochimica et Cosmochimica Acta*, **65**, 3491–3503.

Russell, A.D., Emerson, S., Nelson, B.K., Erez, J. and Lea, D.W. (1994) Uranium in foraminiferal calcite as a recorder of seawater uranium concentrations. *Geochimica et Cosmochimica Acta*, **58**, 671–681.

Schindler, M. and Putnis, A. (2004) Crystal growth of schoepite on the (104) surface of calcite. *The Canadian Mineralogist*, **42**, 1667–1681.

Sturchio, N., Antonio, M., Soderholm, L., Sutton, S. and Brannon, J. (1998) Tetravalent uranium in calcite. *Science*, **281**, 971–973.

Topping, S. and Bruce, S. (2006) A ponderous hazard. *Nuclear Engineering International*, **51**, 28–32.

Vaughan, D.J. and Wogelius, R.A. (2000) *Environmental Mineralogy*. Eötvös University Press, Budapest.

https://doi.org/10.1180/minmag.2012.076.8.24 Published online by Cambridge University Press